DIRECT NUCLEAR HEATING MEASUREMENTS AND ANALYSES FOR STRUCTURAL MATERIALS INDUCED BY DEUTERIUM-TRITIUM NEUTRONS

BLANKET ENGINEERING

KEYWORDS: *fusion reactor, nuclear heating, plasma-facing components*

Y. IKEDA *Japan Atomic Energy Research Institute*
Department of Reactor Engineering, Tokai, Ibaraki 319-11, Japan

A. KUMAR *University of California, Los Angeles*
School of Engineering and Applied Science, Los Angeles, California 90095

C. KONNO, K. KOSAKO, Y. OYAMA, F. MAEKAWA, and H. MAEKAWA *Japan Atomic Energy Research Institute*
Department of Reactor Engineering, Tokai, Ibaraki 319-11, Japan

M. Z. YOUSSEF and M. A. ABDOU *University of California, Los Angeles*
School of Engineering and Applied Science, Los Angeles, California 90095

Received January 28, 1994
Accepted for Publication July 28, 1994

Nuclear heat deposition rates in the structural components of a fusion reactor, have been measured directly with a microcalorimeter incorporated with an intense deuterium-tritium (D-T) neutron source, the Fusion Neutronics Source (FNS) at the Japan Atomic Energy Research Institute (JAERI), under the framework of the JAERI/U.S. Department of Energy (U.S. DOE) collaborative program on fusion neutronics. Structural materials of aluminum, titanium, iron, nickel, molybdenum, and Type 304 stainless steel, along with a ceramic of Li_2CO_3, have been studied with a small-size single probe configuration, subjecting them to D-T neutrons. Heat deposition rates at positions up to 200 mm of depth in a Type 304 stainless steel assembly bombarded with D-T neutrons were measured along with these single probe experiments. The measured heating rates were compared with comprehensive calculations in order to verify the adequacy of the currently available database relevant to the nuclear heating. In general, calculations with data of JENDL-3 and ENDL-85 libraries gave good agreement with experiments for all single probe materials, whereas RMCCS, based on ENDF/B-V, suffered from unreasonable overestimation in the heating number. For Li_2CO_3 with a low heat conduction coefficient, analysis was carried out by using a heat transfer calculation code ADINAT, coupled with the neutron and gamma-ray transport DOT3.5. It was demonstrated that the nuclear/thermal coupled calculation is a powerful tool to analyze the time-dependent temperature change due to the heat transfer in the probe materials. The analysis for the Type 304 stainless steel assembly, based on JENDL-3, demonstrated that the calculation, in general, was in good agreement with the measurement up to 200 mm of depth along the central axis of the assembly. The experimental approach demonstrated in this study clearly showed the feasibility of the calorimeter to measure the nuclear heating for the neutron field where the 14-MeV contribution is relatively small in comparison with the low-energy neutron contribution.

I. INTRODUCTION

The importance of nuclear heating in structural materials has been recognized from the point of view of system design of deuterium-tritium (D-T) fusion reactors. Requirements for reduction of the design margin is stringently addressed from the critical design criteria. The uncertainty of the database relevant to the nuclear

heating is considered as one of the most crucial problems in the designs not only for inboard shielding but also for the plasma-facing component configurations. Many data libraries have been compiled and issued so far to be implemented in the neutron transport code system.[1-6] Adequacy of these data, however, has not been tested due to lack of suitable experimental data.

Since 1989, extensive effort has been devoted to the development of a measuring technique for nuclear heating in the D-T fusion environment in the framework of the Japan Atomic Energy Research Institute/U.S. Department of Energy (JAERI/U.S. DOE) collaboration on fusion neutronics[7-10] at the Fusion Neutronics Source[11] (FNS) at JAERI. The microcalorimetric method, which has been applied in the reactor dosimetry studies,[12-16] has been adopted in the direct measurement of nuclear heating in fusion reactor structural components subjected in D-T neutron fields. This technique provides direct and totally integrated data associated with the heating process by neutrons in the materials. The series of experiments demonstrated the feasibility of the microcalorimetric method for direct nuclear heating measurements, even though the signal was very small in the available D-T neutron source at FNS (Ref. 11), the strength of which was around 3×10^{12}/s.

This study, focusing on structural materials, describes experimental measurements with a "single probe" configuration for aluminum, titanium, iron, nickel, molybdenum, Type 304 stainless steel, and a ceramic of Li_2CO_3. Precise experimental data examination and analysis were performed. The experimental analysis was carried out by using neutron transport codes and comprehensive nuclear data libraries based on JENDL-3 (Ref. 17), RMCCS (Ref. 18), and ENDL-85 (Ref. 19). The time-dependent temperature profiles are analyzed with the ADINAT code,[20] coupling neutron/gamma-ray transport calculations and heat transfer on Li_2CO_3 with a low heat conduction coefficient. Based on the ratio of calculation-to-experiment (C/E) analyses, uncertainty ranges in the kerma factor for D-T neutrons are discussed for the materials tested.

Besides the "single-probe" experiments, nuclear heating distribution in a Type 304 stainless steel assembly was measured. The data in this experimental configuration are expected to be more suitable to validate calculations in the spectrum in the fields where the D-T neutron contribution is less important, and associated gamma-ray and slow neutron contributions are dominant. Measured data up to 200 mm of depth in the Type 304 stainless steel assembly are analyzed by the DOT3.5 calculation with the JENDL-3 nuclear data.

In Sec. II, the technical background and experimental procedure is outlined. Section III gives the experimental results with graphical presentation of nuclear heating. The analytical condition is described in Sec. IV. The discussion of data validation based on the C/E values is given in Sec. V. Section VI summarized the results of this study.

II. EXPERIMENT

II.A. Microcalorimeter for Direct Nuclear Heating Measurement

The microcalorimetric technique comprises two components: the material absorbing the radiation energy and a thermal sensor for detecting the temperature rise due to the absorbed radiation energy. The technique has been applied for ordinary neutron/gamma dosimetry applications and nuclear heat deposition rate measurements in the fission reactor environment.[12-16] The application of this technique in a D-T fusion neutron field, however, required additional considerations, i.e., a very small temperature rise due to the nuclear heating is expected in materials subjected to a neutron flux level from 10^9 to 10^{10}/cm$^2 \cdot$s^{-1}, which is considered a lower limit to generate the nuclear heating signal as long as the available neutron source strength at FNS (Ref. 11) is concerned. A corresponding temperature rise ranging from 10^{-4} to 10^{-5} K/s has been observed in the previous experiments.[7-10] It is critical to detect such a slight signal against the large background due to the ambient temperature change. To meet this critical condition, the following are required: (a) stabilization of the microcalorimeter system, (b) precision of the electric device with low noise, and (c) elimination of the background noise. Even though these conditions are satisfied, there is an inherent heat source due to the applied current on the resistance of the thermal sensor. To minimize such that the macroscopic temperature change is governed by the current source, the slope of temperature change was differentiated by taking derivatives for each subsequent piece of data. In this scheme, the stability of background drift is very essential to realize a good signal-to-noise (S/N) ratio. No heat flow in the probe material is assumed. This assumption is valid if the size of the material is small enough to make no difference in the temperature gradient and/or the material has a high thermal conductivity coefficient. It is also commonly understood that the heat transfer between the probe and ambient materials through convection and conduction is very slow in speed if the system is well stabilized with thermal equilibrium. In a short time span, it could be assumed that the heat transfer has a constant change. The static background noise, however, should be kept as low as possible. Eliminating the slow or constant component, the differentiation of temperature gives better S/N ratios in the range of a factor of ten or more in comparison with the direct observation of the slope of the temperature rise.

II.B. Experimental System

The experiment was divided into two parts. The first experiment dealt with single-probe materials subject to D-T neutrons directly. Structural materials of aluminum, titanium, iron, nickel, molybdenum, and

Type 304 stainless steel along with a ceramic of Li_2CO_3 were tested mainly to provide nuclear heating data for verifying the kerma data for the 14-MeV neutrons. The material properties are listed in Table I. The second part is the measurement of the heat deposition rate distribution in a Type 304 stainless steel assembly. Hereinafter we call the first one the "single-probe experiment" and the second one the "Type 304 stainless steel assembly experiment." A more detailed description on the whole experimental procedure is documented in the joint report under the JAERI/U.S. DOE collaboration.[22]

II.C. Instrumentation

II.C.1. Single-Probe Configuration

A block diagram of this system for nuclear heating is shown in Fig. 1. The D-T neutron source using a rotating target at FNS (Ref. 11) was used to bombard the probe materials. The probe materials were put in a vacuum chamber suspended with thick carbon papers. The distances of the probes from the neutron source position ranged from 3.5 to 4.5 mm. The schematic cross-sectional view of the microcalorimeter is given in Fig. 2. The vacuum chamber was covered with a layer of polystyrene foam to insulate the ambient change of room temperature. This configuration minimizes the thermal conduction and convection from the surrounding area. The following two types of thermal sensors were used: two thermistors [(TM) with 10 kΩ] placed at the front and rear surface of the probe and a platinum resistance thermodetector [(RTD) with 100 Ω] attached on the side. All metal probes had a cylindrical geometry with ~20-mm diameter and 20-mm height, the axis of which aligned to the direction from the neutron source. The size of the Li_2CO_3 probe was 51 × 51 × 51 mm^3. The probe was supported by thin carbon papers in order to reduce the thermal conduction. The sensors were contacted directly on the probe materials with the use of a small piece of organic tape. The sensors were connected by thin wires with voltmeters. The four pole measurement was performed for RTD with less resistance to mitigate the effect of the resistance of connecting wires. The coefficients of the sensors for the temperature change were 2.04×10^{-3} K/Ω and 2.53 K/Ω for the TM and the RTD, respectively. The temperature rise of 10^{-5} K/s corresponded to a voltage change of 5×10^{-8} V and 4×10^{-6} V when 10-μA and 1-mA currents were applied on 10-kΩ and 100-Ω resistances, respectively, resulting in the last one or two digits change of the nanovoltmeters used (Keithly-181 and -182, and Solatron-7081). This means that the stability of the system for the ambient temperature change as well as the self-heating is very crucial in order to observe a meaningful signal.

II.C.2. Type 304 Stainless Steel Assembly Configuration

Figure 3 illustrates the cross-sectional view of the assembly made of the Type 304 stainless steel core region, side Li_2CO_3 enclosure, and polyethylene insulator. As we can see, the D-T neutron source was not enclosed with the materials. Thus, a large number of slow neutrons reflected from the wall of the target room were expected to impinge onto the assembly at the front and rear surfaces. From the side, it was mitigated by the Li_2CO_3 and polyethylene layers. The nominal size of the core Type 304 stainless steel was 357 × 458 × 458 mm^3. Cubicle blocks of Type 304 stainless steel with unit dimensions of 51 × 51 × 51 mm^3 were contained in a Type 304 stainless steel box and stacked with each other. The outer regions of the side with respect to the d^+ beam direction were covered with Li_2CO_3 bricks. The supporting frame was made of Li_2CO_3, which was used in the Phase-II series of experiments of the JAERI/U.S. DOE collaboration.[23,24] The front surface was placed in close vicinity to the D-T neutron source in order to maximize the neutron flux levels inside the Type 304 stainless steel core, resulting in a high S/N ratio.

TABLE I

Material Properties and Dimensions of Probes

Materials	Specific Heat[a] $(J/g \cdot K)^{-1}$	Conductance $(W/m \cdot K)^{-1}$	Density (g/cm^3)	Dimension (mm)
Aluminum	0.900	235	2.70	20 diam × 20
Titanium	0.527 (0.528)[b]	22	4.51	21 diam × 20
Iron	0.435 (0.460)	84	7.87	20 diam × 20
Nickel	0.444 (0.440)	91	8.90	21 diam × 20
Molybdenum	0.248 (0.255)	135	10.22	21 diam × 20
Type 304 stainless steel	0.548	16.3	7.93	20 diam × 20
Li_2CO_3	0.879 (---)	1 to 5	1.82	50 × 50 × 50

[a]Value at 300 K.
[b]Values in parentheses were taken from Ref. 21.

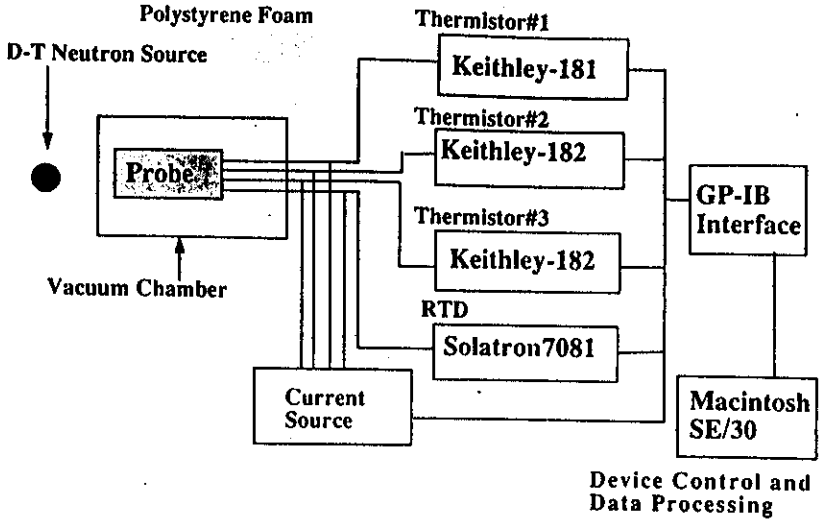

Fig. 1. Block diagram of direct nuclear heating measurement with a microcalorimeter.

The idea for applying the Type 304 stainless steel block itself as the probe material was based on the assumption that heat flow is not significant in the short period of 30 to 100 s for the data sampling. The thermal insulator of thin paper was attached on each block. For the first three blocks, the TM (10-kΩ) sensors were attached on the surface closer to the D-T neutron source, and thin lead wires were extracted through the thin space between blocks. On the side of the fourth block at a depth range of 170 to 220 mm, a 100-Ω RTD was attached and the leading wire was extracted also utilizing the small space between blocks. The extracted wires were directly connected with the voltmeters of Keithly-181, -182, and Solatron-7081.

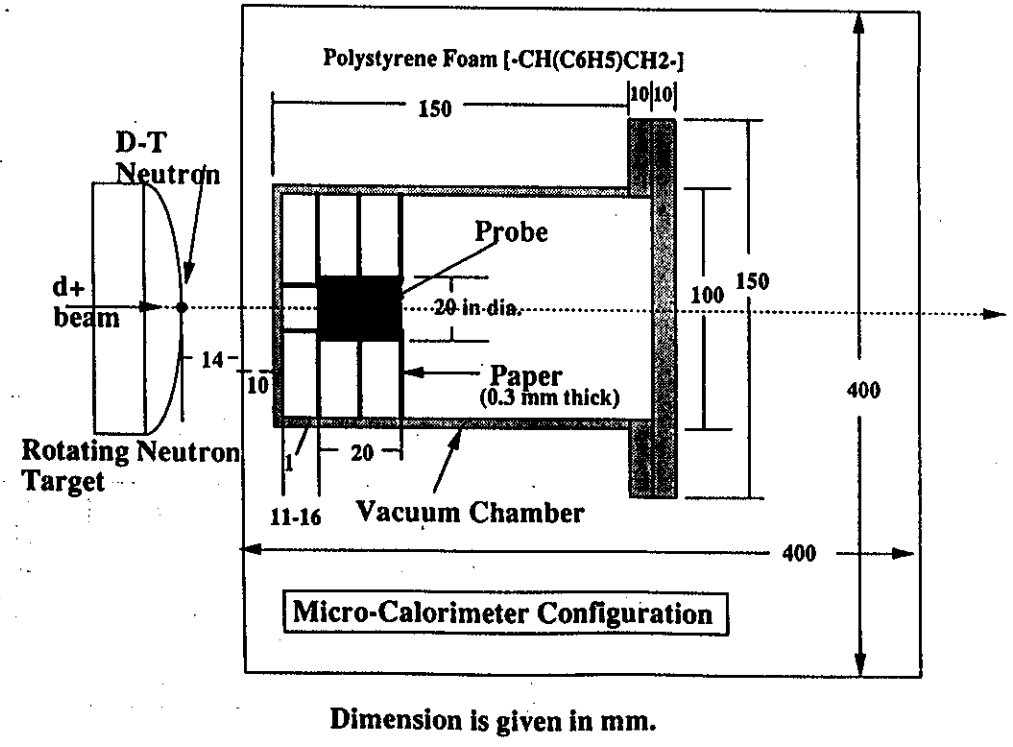

Fig. 2. Cross-sectional view of the microcalorimeter and experimental configuration.

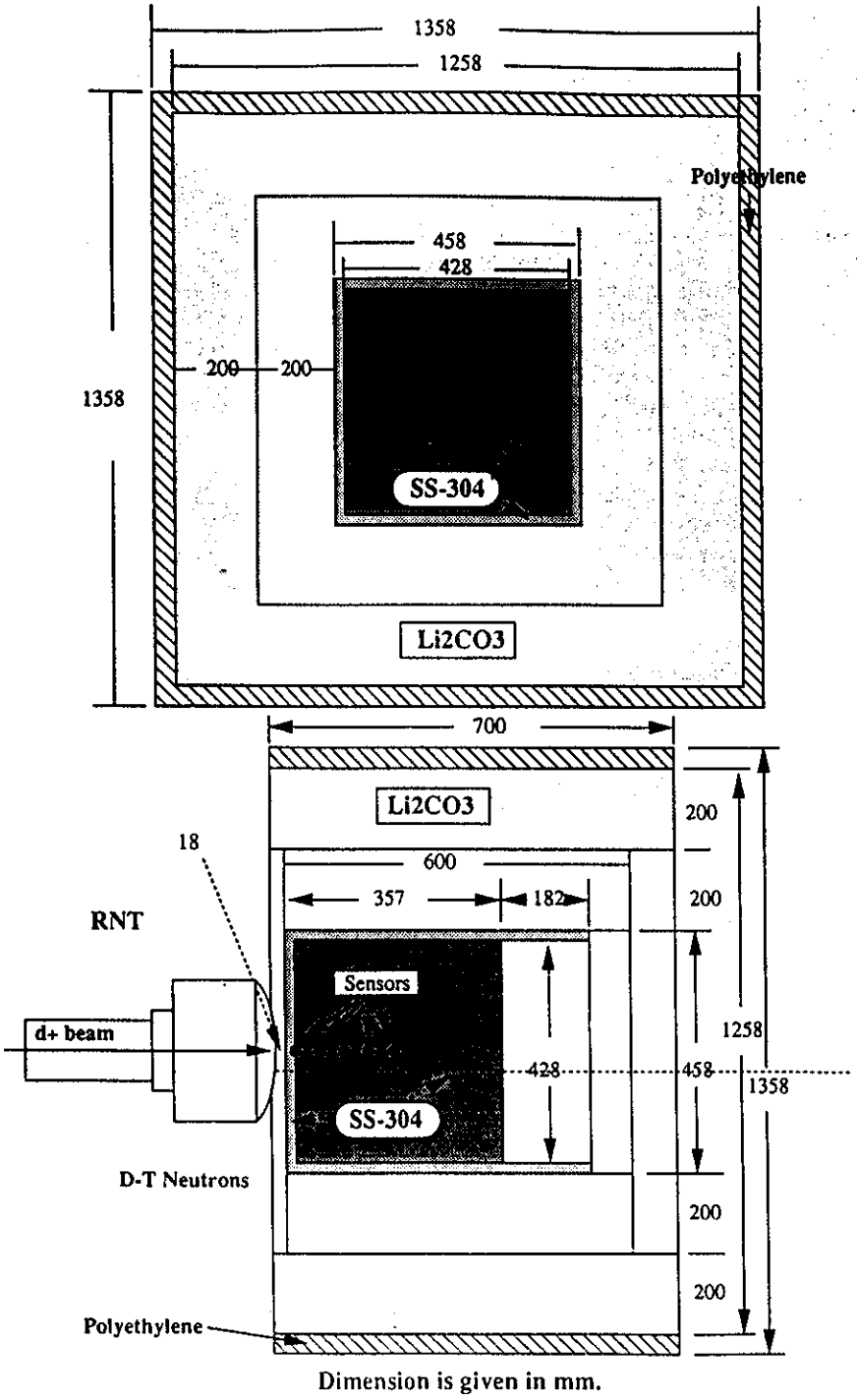

Fig. 3. Cross-sectional views of the Type 304 stainless steel assembly (RNT = rotating neutron target).

II.D. Neutron Source and Bombardment of Probe

II.D.1. Single-Probe Experiments

The D-T neutrons were generated by bombarding a tritiated metal target with a deuteron beam of 350 kV and 20 mA. The absolute neutron yield was monitored by a ^{232}Th fission chamber calibrated by the associated alpha-particle counting method.[25] The calorimeter was irradiated with neutrons over a time space in the range of 3 to 5 min. Before irradiation, we had to wait to stabilize the thermal probe system. Sometimes, a preheating of the probe was required to facilitate the procedure. A constant current was applied to the resistance

thermal sensors throughout the irradiation to detect the signal during the irradiation. Thin niobium foils were placed in the front and back sides of the probe to measure the exact neutron flux during the irradiation. The location of the probe was deduced from the D-T neutron source strength obtained by the fission chamber and the neutron flux derived by using the reaction rate of $^{93}Nb(n,2n)^{92m}Nb$ assuming a cross section of 459 mb at 14.9 MeV (Ref. 26).

II.D.2. Type 304 Stainless Steel Assembly Experiment

Sampling times of 30 to 100 s longer than that of 10 s in the single-probe measurements were applied to increase the effective temperature rise output. If the adiabatic condition was valid, we should have a larger temperature rise. This scheme, however, introduced another uncertainty in the determination of the realistic temperature due to the heat flow in the relatively large probe zone and relatively large gradient of the heating rate. The D-T neutron source strength was identical to those for the single-probe experiments. The same long pulsed neutron operation was applied to discriminate the background drift of slow components due to radiation, heat conduction through both cable lines, and paper insulator attached upon adjacent Type 304 stainless steel blocks.

III. EXPERIMENTAL RESULTS

III.A. Graphical Representation of Signals Due to Nuclear Heating

III.A.1. Single-Probe Experiments

III.A.1.a. Aluminum. Figure 4 shows the derivatives of the temperature change. This case was the worst in terms of the stability of the temperature in the system. The temperature at the probe suffered from a large change of the ambient temperature. Positive values of the derivatives as shown in Fig. 4 indicated a strong heat flow into the probe through the wires of the sensor. The responses to the D-T neutron pulses appear as shown in Fig. 4, superimposed on the drift-line of the slow component with the winding curve. The response to the long neutron pulse for 30 min suffers from a large drift during the irradiation. However, the responses to short pulses for 5 min each give a clear rise in the temperature. It was demonstrated that the derivative is very effective to obtain the signal of the nuclear heating.

III.A.1.b. Titanium. The data of the temperature change and its derivatives are shown in Figs. 5a and 5b, respectively. On the contrary to the aluminum case, the temperature change exhibits a descending profile. However, the range of the change is one order of magnitude less than in the aluminum case. It suggests that overall stability was much better than that in the aluminum

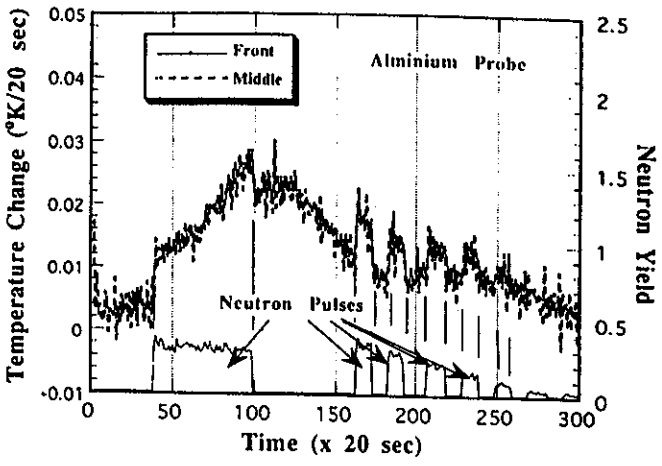

Fig. 4. Derivatives of the temperature change in the aluminum probe due to D-T neutron irradiation.

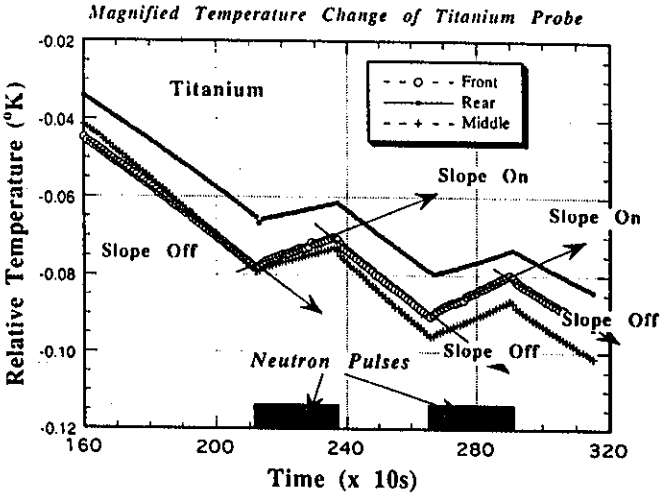

Fig. 5a. Temperature changes in the titanium probe.

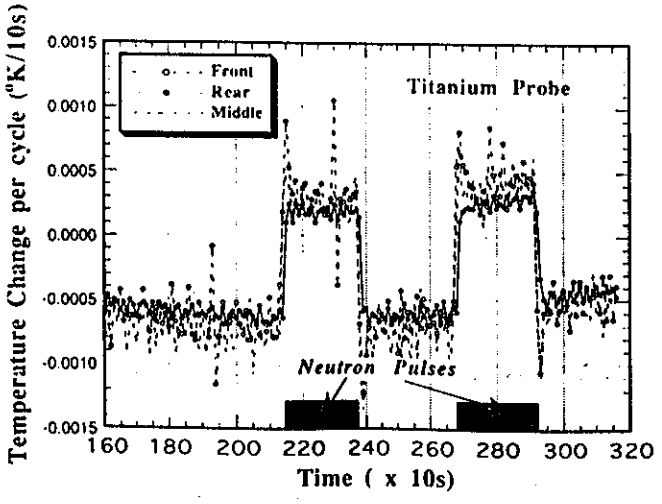

Fig. 5b. Derivatives of the temperature change in the titanium probe due to D-T neurton irradiation.

measurement. As a result, there are clear changes in the slope of the temperature. At the start of the neutron pulses, the temperature starts to increase, and at the end of the neutron pulse, it continues to decrease as the similar slope before the neutron pulse. The difference in the absolute temperatures between thermistors at the front and rear of the probe may be caused by the different heat flow rate through the wires. However, the reduced slopes to the neutron pulses, correspond reasonably to the difference in the temperature rises at the front and the rear. As the titanium has relatively low thermal conductivity in comparison with other common metallic materials, there should be a difference in the rate of temperature rise according to the neutron flux gradient. Figure 5b, showing the derivatives of the temperature change as a function of time, gives the difference more explicitly. The drift line corresponding to the slow component is almost constant. This is due to the better thermal stability in the system as described. It is clearly observed that the rate of temperature rise at the front, at the beginning of the neutron pulse, is appreciably higher than that at the rear. The temperature rise measured with RTD, which was assumed to correspond to the data in the middle of the probe, is almost flat through the irradiation. The rates at the front and rear approach to almost the same value at the end of irradiation. This is explained by the equilibrium of the temperature through the heat transfer in the probe.

III.A.1.c. Iron. Figure 6 gives the derivatives of the temperature change. The responses due to the neutron pulses are clearly obtained. In this case, the difficulty in the large change in the drift line was mitigated. A meaningful difference in the values between front and rear is not observed in this case. A factor of four higher thermal conductivity than titanium mitigated the heat transfer problem.

III.A.1.d. Nickel. Figures 7a and 7b correspond to the temperature change and its derivatives, respectively. As shown in Fig. 7a, a very clear temperature profile is observed. An almost ideal case was realized by achieving a good thermal stability in the probe system. One could extract very easily the temperature rise due to the nuclear heating from the difference in the slopes before and after neutron irradiation. The derivatives of the temperature change, as shown in Fig. 7b, however, were used to derive the net response to the neutron irradiation. It should be noted that the fluctuation of the drift line is much smaller than those observed in the aluminum and iron cases. In particular, the data taken with Keithly-182 offered very small fluctuations throughout the measurements.

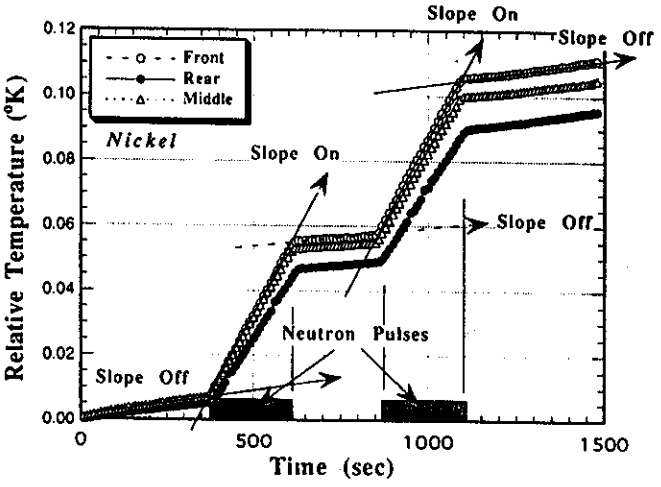

Fig. 7a. Temperature changes in the nickel probe.

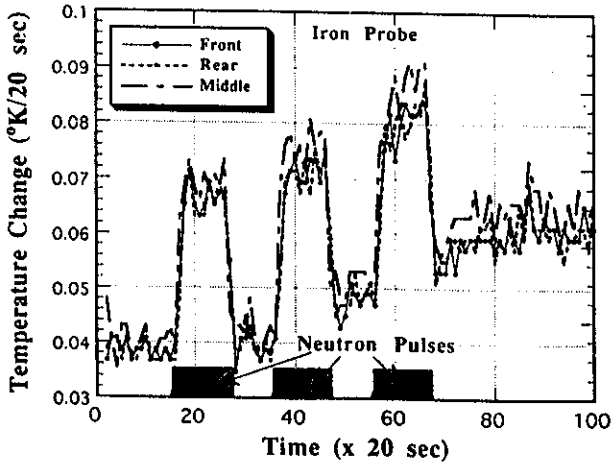

Fig. 6. Derivatives of the temperature change in the iron probe due to D-T neutron irradiation.

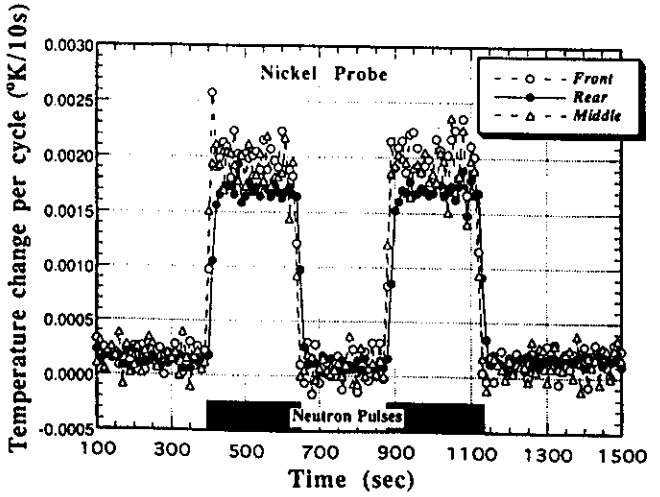

Fig. 7b. Derivatives of the temperature change in the nickel probe due to D-T neutron irradiation.

III.A.1.e. Molybdenum. The temperature change and the derivatives are plotted in Figs. 8a and 8b, respectively. The changes in slopes corresponding to the neutron irradiation are also clearly exhibited as shown in the titanium and nickel cases. The flat top profile of derivatives, given in Fig. 8b, indicated the high thermal conductivity of molybdenum. In fact, the conductivity of molybdenum. is the largest among those of metallic materials studied except aluminum.

III.A.1.f. Type 304 Stainless Steel. Although the change in the slopes according to the neutron pulses were observable, the measurement suggested that the overall temperature profile was governed by the external heat flow. Performing the derivation, clear responses are obtained as shown in Fig. 9.

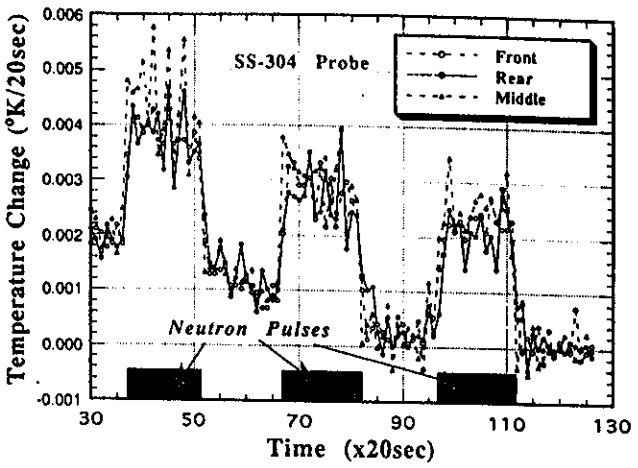

Fig. 9. Derivatives of the temperature change in the Type 304 stainless steel probe due to D-T neutron irradiation.

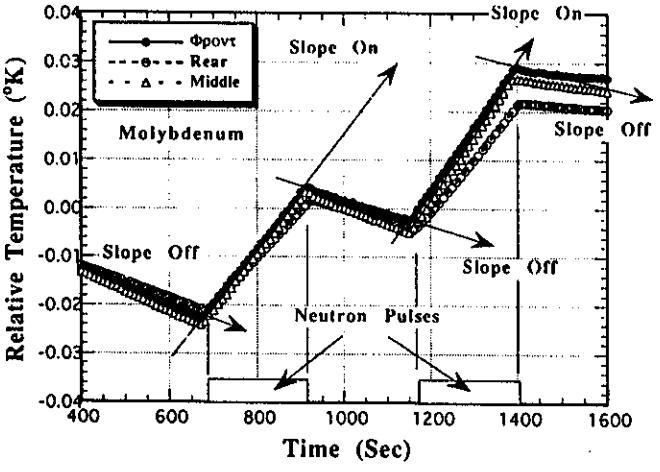

Fig. 8a. Temperature changes in the molybdenum probe.

III.A.1.g. Lithium Carbonate. Figure 10 gives the derivatives of the temperature change in the Li_2CO_3 probe. As observed in the figures, a higher value in the slopes of the temperature rise was always found for the data on the front in comparison with the rear data. In general, a material with lower thermal conductivity gives a higher ratio. This is reflected by the thermal conduction problem in the short integration time of 10 s (sampling time). Since the probe was exposed to a strong D-T neutron flux at the close vicinity of the neutron source, a steep gradient of nuclear heat deposition along the axis of the probe makes heat flow in the material. In the integration time for 10 s, equilibrium could not be accomplished, so that slight imbalance was expected. This situation is clearly observed in Fig. 10. A fast and

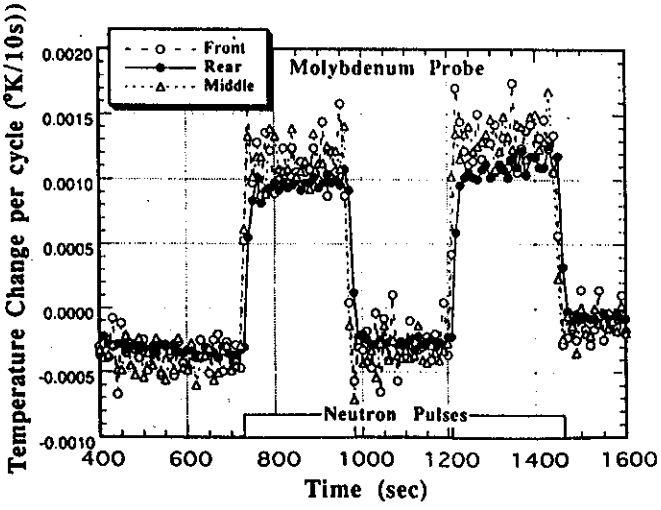

Fig. 8b. Derivatives of the temperature change in the molybdenum probe due to D-T neutron irradiation.

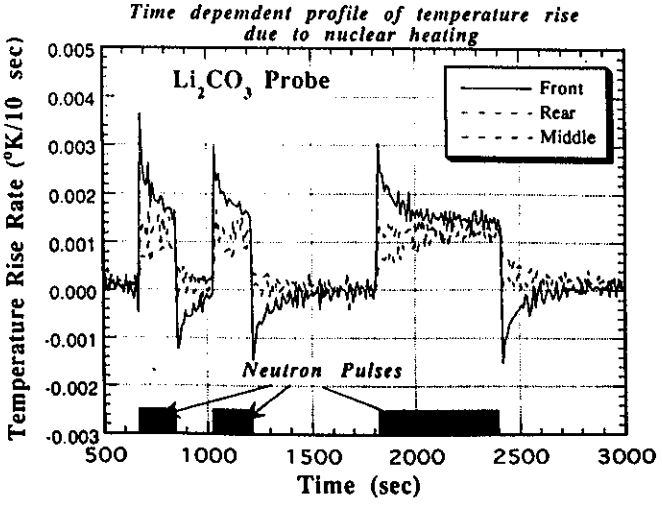

Fig. 10. Derivatives of the temperature change in the Li_2CO_3 probe due to D-T neutron irradiation.

larger rise on the front and slow and smaller rise on the rear were detected at the beginning of the neutron shot. The data gradually approached to an identical value at the end of the irradiation. In particular, clear overshoot and undershoot of resistance change on the front as shown in Fig. 10 indicated thermal conduction phenomena at the boundary for the pulsed heating source. The previous experiment adopting 20 to 30 s for the integration time mitigated the imbalance in temperature equilibrium at both ends of the probe. Contrary to TM, RTDs inserted in the middle of the probe from the side perpendicular to the axis show flat response during the irradiation as shown in Fig. 10. Especially in the material probe of Li_2CO_3 with low thermal conductivity, there was a recognition of more enhanced time dependency in the heat flow in the probe materials during irradiation. This figure shows explicitly the process of equilibrium of temperature according to the gradient of the heat deposition rate distribution.

III.A.2. Type 304 Stainless Steel Assembly Experiment

The derivatives of temperature changes for the Type 304 stainless steel block detectors are shown in Fig. 11. The data at the position closest to the D-T neutron source display the highest values with strong overshoots and undershoots at the beginning and end of the neutron pulse irradiation, respectively. This profile is very similar to that observed in the Li_2CO_3 probe. Considering the relatively low thermal conductivity of Type 304 stainless steel and the steep gradient of the neutron flux over the large block detector with 51-mm length, the variation in the derivatives during irradiation is explained by heat transfer from the front to the rear sides. This effect due to the heat flow, though it was not prominent, was observed in the data at the second position. The neutron flux gradient at this position is expected to be much smaller than that at the first probe. At the third position, an almost flat distribution is detected. Although the data at the last position at 210 mm, measured with RTD is identical to the background drift line, there are slight rises in the average. Throughout the Type 304 stainless steel assembly experiments, a longer cycle time of 50 s was adopted in order to increase the temperature rise in assuming the adiabatic condition within the probe.

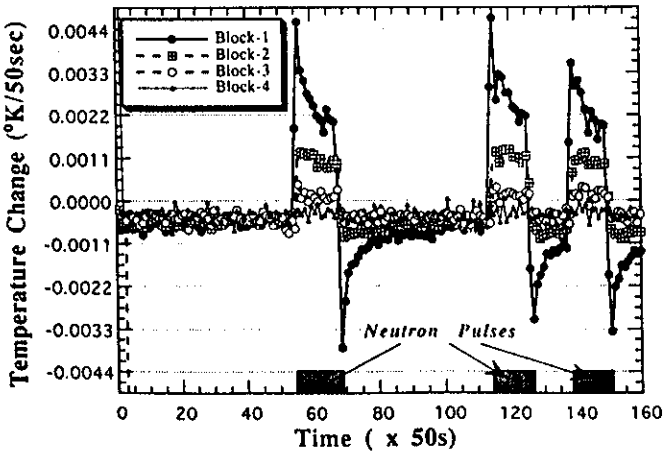

Fig. 11. Temperature changing rates in the Type 304 stainless steel probes along the central axis of the Type 304 stainless steel assembly.

III.B. Nuclear Heating Rate Reduction

The temperature rise as given in the previous section was obtained by multiplying the resistance changes with the conversion coefficient C_α for each thermal sensor, TM (2.04×10^{-3} K/Ω) and RTD (2.53 K/Ω). The temperature rise per source neutron T is given as

$$T = C_\alpha \cdot R/t \cdot Y_n^{-1} \text{ (K/s·source neutron}^{-1}\text{)} ,$$

where

t = cycle time for data acquisition (s)

Y_n = source neutron strength (s^{-1}).

The experimental data for the temperature rises for the single probe materials were given as an average between the front and rear for the thermistor, averaging the data of all shots. For the Li_2CO_3, the data derived from the RTD measurement were employed, because a large uncertainty in averaging the data of the front and the rear was expected from the thermal equilibrium point of view. On the other hand, as described in the Type 304 stainless steel block probes with larger sizes, the data at the position of the thermal sensors seem most suitable from the spatial resolution point of view.

For the determination of the nuclear heating rate with the Type 304 stainless steel block detector, as regards the spatial resolution, the data at the starting moment of the neutron pulse were assumed to correspond to the nuclear heating. The data during irradiation, as described, suffered from heat transfer, giving less value than that at the initial point. From the curve of the derivatives, it was judged that the last point was not good in equilibrium. The nuclear heating rate is erg per gram per source, then, was derived by applying the number of the specific heat[21] of each material given in Table I.

III.C. Experimental Errors

The self-heating driven by the joule heat in the resistance of the thermistor sensor gives a constant heating load, which contributes a constant change of the temperature. If the weight of the 10-kΩ thermistor sensor is assumed to be 10^{-3} g, the heat generation with 10 μA was equivalent to 10^{-3} W/g, resulting in a much higher rate than that produced in the nuclear heating

process ranging from 10^{-4} to 10^{-5} W/g. The other factor to be considered was the contribution to the temperature change from heat conduction even though it was small and slow. Even in the circumstance with good air conditioning, a change of 10^{-2} K is unavoidable. This change makes a steep gradient in the temperature between the probe and the circumstance in comparison with the temperature change due to the nuclear heating. The overall fluctuation of the drift line was, as a result, governed by the constant self-heating and the slow component due to the ambient temperature change in the room along with electrical noise (it may be some timing effect). As the signal of nuclear heating is superimposed on that slow component, the stability of the drift-line determines the error for the nuclear heating derivation. The nominal error due to the fluctuation of the drift-line ranged from ±3 to 5% with respect to the net nuclear heating signal in a well-stabilized condition. If the stability of the system was not sufficient, the error ranged from ±10 to 15% with respect to the net nuclear heating signal.

As mentioned earlier, the distance of the probe from the neutron source was determined by using the neutron source strength and the reaction rate measurement of niobium foil activation. A change of 1 mm in the distance of 37 mm made a maximum change of 4% in the heating rate as long as the calculation of JENDL-3 was concerned. Thus, the uncertainty in the determination of distance should be taken into account as the experimental error. In this data processing, we assumed adiabatic thermal insulation, no thermal convection, and conduction and radiation between the probe and the environment. The validity of this assumption was examined by the ADINAT calculations, which considered all the heat flow process and gave a negligibly small contribution.

Other factors of error sources were the source neutron yield, coefficients of the thermal sensors, and specific heat data. The experimental errors and uncertainties considerations are summarized in Table II.

TABLE II

Experimental Errors and Uncertainties

Items	Range
Neutron flux determination	
Probe positioning	±4%
Nb($n,2n$) reaction rate	±2.5%
Cross section	±3%
Absolute neutron yield	±2%
Net temperature rise derivation	
Fluctuation of drift-line	<±5%[a]
Determination of background	<±5%[a]
Conversion coefficient of sensors	±1%
Volume averaging procedure	±2%[b]
Heat loss/gain through conduction, convection, and radiation	±2%[c]
Specific heat data	±2%[d]
Overall	<±10

[a]For the aluminum, iron, and Type 304 stainless steel cases, the errors assigned were ±15, ±10, and 10%, respectively.
[b]The error was tentatively assigned from the difference of data at the front and the rear.
[c]The error was tentatively given.
[d]There is no explicit error for the specific heat data in the literature. The uncertainty is considered from the difference in the values taken from the different sources.

IV. ANALYSIS

The neutron and gamma-ray transport calculations were carried out by using the two-dimensional code DOT3.5 (Ref. 27) and the three-dimensional code MCNP (Ref. 18) with nuclear data libraries, including FUSION-J3 (Ref. 28) based on JENDL-3 (Ref. 17) for DOT3.5 and RMCCS (ENDF/B-V) (Ref. 18) for MCNP. Both calculations modeled the experimental system as precisely as possible, including the rotating neutron target structure, the microcalorimetric system, and the target room. In the DOT3.5 calculation, a P_5S_{16} approximation was used for the r-z model and the first collision source was calculated by the GRTUNCL code. The kerma factors of neutron and gamma ray for the DOT3.5 calculations were generated from the JENDL-3 by using the NJOY processing code[29] and from DLC-99 (Ref. 30) by the energy balanced method,[31] respectively. The heating numbers of the libraries with MCNP, i.e., RMCCS (Ref. 18), and ENDL85 (Ref. 19), were used for the MCNP calculations. The calculated heating rate in each material was converted to the temperature rise in the unit of kelvin per source neutron to be compared with the measurement. In this analysis, we didn't treat time-dependent thermal conduction during the finite irradiation time. The value to be compared with the experiment was the derived averaged data over the entire volume of the probes except for Li_2CO_3. The Li_2CO_3 probe has a considerably low thermal conduction so that the time-dependent profile should be taken into account. Comparison of the measurement and calculation was performed in the dimensions of erg per gram per source neutron of 10^{12}/s. The specific heat (joule per gram per kelvin) was used to derive the heating rate from the measured data of the temperature rise in kelvin.

The time-dependent profile of the temperature rise due to heat transfer in the probe medium of Li_2CO_3 was analyzed with the ADINAT code,[20] which couples the heat source calculation associated with DOT3.5 for neutron and gamma-ray transport and the heat transfer phenomena in terms of convection, conduction, and radiation of the system. The initial temperature of the system was assumed to be the room temperature of

25°C. Neutron pulses simulating exactly the same experimental condition were put in the calculation. FUSION-J3 (Ref. 28) was used for the DOT3.5 transport calculation and the successive nuclear heating calculation, with the two-dimensional r-z model. As the vacuum chamber was used, no convection was treated.

V. DISCUSSION

V.A. Single-Probe Experiment

V.A.1. 14-MeV Neutron Sensitivity

To give the general idea of how much the 14-MeV neutrons contribute to the total neutron heating, Fig. 12 gives a calculated product of the neutron spectrum at the middle of the probe and the neutron kerma for nickel, as an example. This figure demonstrates that 14-MeV neutrons dominated the total neutron heating. Based on this calculation, the fraction of more than 96% is originated by the 14-MeV neutrons. This implies that these data are effective for the verification of the neutron kerma data at the 14-MeV region. There is uncertainty caused by the gamma-ray fraction. As the preliminary analysis shows in Table III, external gamma-ray contributions are <10% for almost all materials except aluminum. The contribution of external sources was calculated by putting a negligibly small piece of material at the same location of the center of the probe instead of the probe. In this case, the heat production by the associated gamma-ray that originated in the probe materials could be neglected. Although the external gamma-ray heating rate is not exactly the same as the calculation with the actual probe size, it can be assumed that they give the same magnitude of fractional contributions to the total. The uncertainty due to the error of the external gamma-ray source, as a result, falls in <5% even if the error of gamma-ray spectrum flux is assumed to be ±50% in the calculation.

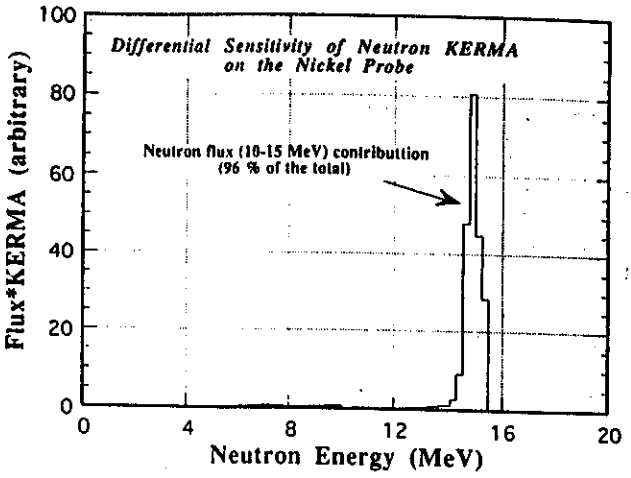

Fig. 12. Differential sensitivity of the nuclear heating in a nickel probe associated with neutrons. The sensitivity is a calculated product of the neutron spectrum at the middle of the probe and the neutron kerma for nickel.

V.A.2. Material Wise Discussion

Table IV gives a summary of ratios of C/E corresponding to all kerma libraries tested here. The calculations based on nuclear data libraries of JENDL-3, RMCCS, and ENDL-85 are, hereafter, to be denoted as JENDL, RMCCS, and ENDL-85, respectively. Materialwise discussion is as follows:

V.A.2.a. Aluminum. JENDL underestimated the experiment by 20%. Taking into account the experimental error of ±20%, the agreement seems acceptable. RMCCS, on the other hand, largely overestimated the experiment by 80%. Even considering the large experimental error, this range of overestimation requires further examination of data processing for RMCCS. ENDL-85 gives the best results among the libraries

TABLE III

Calculations of Nuclear Heating Contributions by Neutron, Gamma Ray, and External Gamma Rays*

Material	Neutron	Gamma-Ray Total	External Gamma Ray	Total ($n+\gamma$)
Aluminum	2.014E−10[a] (86.5)[b]	3.145E−11 (13.5)	1.616E−11 ((51.4))[c]	2.329E−10
Titanium	1.015E−10 (48.8)	1.064E−10 (51.2)	3.820E−11 ((35.9))	2.079E−10
Iron	1.755E−10 (70.4)	7.363E−11 (29.6)	2.384E−11 ((32.4))	2.491E−10
Nickel	2.554E−10 (69.6)	1.113E−10 (30.4)	3.934E−11 ((35.3))	3.667E−10
Molybdenum	3.425E−11 (22.0)	1.218E−10 (78.0)	4.540E−11 ((37.3))	1.561E−10
Type 304 stainless steel	3.337E−10 (73.3)	1.216E−10 (26.7)	2.863E−11 ((23.5))	4.553E−10
Li_2CO_3	5.823E−10 (94.5)	3.385E−11 (5.5)	2.925E−11 ((86.4))	6.162E−10

*Nuclear heating rate is obtained as the volume averaged in the unit of erg per gram per source.
[a]Read as 2.014×10^{-10}.
[b]Values in parentheses give the fractional contribution in percent to the total.
[c]Values in double parentheses give the fractional contributions by external gamma-ray flux in percent to total gamma rays.

TABLE IV

C/E Summary for the Single-Probe Experiment

Material	JENDL	C/E RMCCS	ENDL-85
Aluminum	0.80 ± 0.19[a]	1.78	1.03
Titanium	0.99 ± 0.08	1.06	1.04
Iron	1.20 ± 0.15	1.32	1.21
Nickel	0.99 ± 0.08	1.3	1.21
Molybdenum	1.12 ± 0.06	0.84	0.96
Type 304 stainless steel	1.02 ± 0.15	1.12	0.97
Li_2CO_3	1.00 ± 0.10	0.98	---

[a]Experimental errors are considered. The same relative error should be associated with the values for RMCCS and ENDL-85.

tested. According to the small fraction of the external gamma-ray contribution to the total as shown in Table III, those results imply the validation of the kerma factor for 14-MeV neutrons.

V.A.2.b. Titanium. All calculations are in good agreement with measurements giving the C/Es a range from 0.99 to 1.06. As shown in Table III, there is, however, a considerable amount of external gamma-ray contribution of ~18% to the total heating rate. Also, note that the fraction of the gamma-ray is larger than that of the neutron. As the experimental error was less than ±10%, the kerma data for the single-probe configuration seem adequate. It is strongly recommended to perform further experimental validation for the kerma data, in particular, in a neutron field with different sensitivities for both neutrons and gamma rays.

V.A.2.c. Iron. According to the JENDL calculation given in Table III, neutrons contribute 70% to the total response. The external gamma-ray fraction is <10% of the total. All calculations overestimated the measurement by 20 to 30%. This range seems to be too large to be neglected even though the experimental error of ±13% is taken into account. As iron is the most essential structural material, it is urgently required to validate the heating data as well as the gamma-ray production cross sections of iron. To discriminate the gamma-ray contribution, an additional experiment using probes with larger sizes is suggested.

V.A.2.d. Nickel. The fractions of neutrons and gamma-rays to the total are similar to those of iron. JENDL gives an excellent agreement with the experiment. Since the experimental error is less than ±10%, the adequacy of the calculation with JENDL is assured as long as this single probe configuration is concerned. RMCCS and ENDL-85 overestimate the experiment by 30 and 21%, respectively. Urgent examinations not only for kerma data of each library, but also neutron and gamma-ray transport calculations based on ENDF/B-V are needed.

V.A.2.e. Molybdenum. The contribution of gamma rays dominates the total heating rate, according to Table III. As the materials with higher atomic number tend to have a large gamma-ray absorption coefficient, this large contribution of 78% to the total is reasonably understood. JENDL slightly overestimates the measurement by 12%. In this case, the experimental error is very small being ±5%. Therefore, the source of the overestimation should be examined even though it is small. In contrast to JENDL, RMCCS underestimates the measurement by 15%. ENDL-85 gives the best agreement with the measurement.

V.A.2.f. Type 304 Stainless Steel The neutron and gamma-ray fractions to the total are identical to those of iron as shown in Table III. All calculations are in good agreement within the experimental error of the measurement. This result suggests that the adequacy of the heating data in the libraries could be assured within ±15% for the neutron field close to the first wall. Furthermore, the present results suggest that the overall prediction accuracy including the transport calculation is in a high confidence level because the configuration with the vacuum chamber surrounding the probe, made of the same Type 304 stainless steel, offered a better simulation of the neutron and gamma-ray field.

V.A.2.g. Lithium Carbonate. The C/E values of both JENDL and RMCCS are close to 1.0. This result indicates the adequacy of the data for heating numbers, i.e., kerma factors as long as the averaged value over the entire volume of the probe is concerned. As shown in Fig. 10, however, a more precise analysis should be required by taking into account the time dependency of the temperature change at the front and the rear positions during irradiation.

The Li_2CO_3 probe made by sintering the Li_2CO_3 powder was effectively the lowest Z-material among the materials tested. This reflected the low gamma-ray contribution of 5.5% to the total heating as shown in Table III. As is commonly known, the thermal conductivity of the ceramic is extremely low in comparison with ordinary metallic materials. Even though the conductivity is low, a duration for 10 s was not enough to neglect the heat transfer if the gradient of the temperature was steep. Time-dependent profiles of change in temperature rise rates in Li_2CO_3 were analyzed with a heat transfer code, ADINAT (Ref. 20), which was coupled to the neutron and gamma-ray transport calculation by DOT3.5. As the thermal conductivity for the Li_2CO_3 was not well characterized, a parametric study changing the coefficient of thermal conductivity in the range from 0.5 to 5 $W/min \cdot K^{-1}$ was used, and time-dependent profiles were directly compared with the measurement. Figure 13 shows the calculated time-dependent changes using thermal conductivity coefficients of 0.5, 1.0, and 5.0 $W/min \cdot K^{-1}$, respectively, along with the measured data. It is remarkable that the calculation represents clearly the measurements for the profile of responses

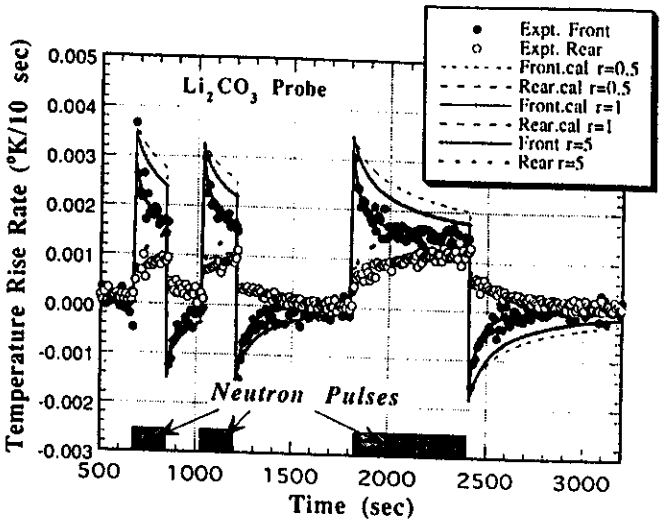

Fig. 13. Comparison of calculations by ADINAT with different thermal conductivity coefficients for the Li_2CO_3 probe with the measurement. The neutron and gamma-ray fluxes were calculated by DOT3.5 with FUSION-J3.

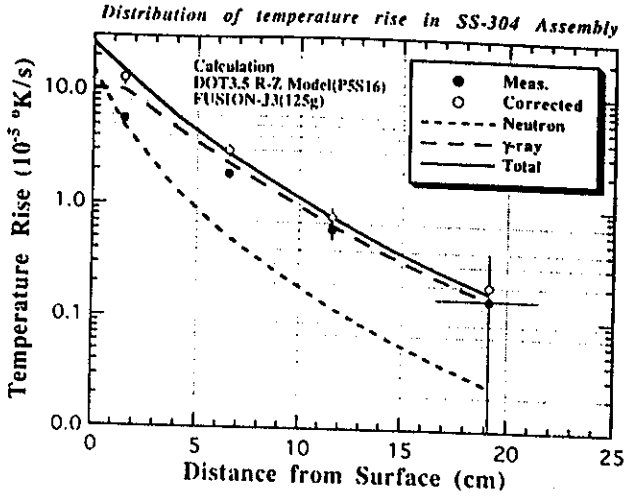

Fig. 14. Measured and calculated nuclear heating distribution in the Type 304 stainless steel assembly.

with strong overshoot and undershoot at the front and slow increase and decrease at the rear, at the beginning and end of the neutron pulses. The calculation with a thermal conductivity coefficient of 5.0 W/min·K^{-1} gives the best fit to the measurement. This result demonstrates that the time-dependent analysis with ADINAT is very effective for the nuclear heating process in the material probe with low thermal conductivity, in which the flux distribution is steep, resulting in a strong heat transfer according to the large gradient of temperature.

V.B. Type 304 Stainless Steel Assembly Experiment

The heating rates were derived from the measured temperature rises at the beginning of the neutron pulses at positions of 15, 65, and 115 mm, and in a range of 165 to 215 mm. The experimental data are plotted in Fig. 14 along with the calculation by DOT3.5 with FUSION-J3 (Ref. 28). The neutron and gamma-ray fractional contributions are given separately in Fig. 14 in addition to the total heating rate. Although both the measurement and the calculation show descending heating profiles as the depth increases, the calculation gives steeper distributions than the measurement at the region close to the neutron source. As shown before, the temperature changing rate in the Type 304 stainless steel block has a strong time dependency profile as observed in the data of the Li_2CO_3 probe. The profile indicated that there is a fairly large amount of heat flow according to the steep flux gradient through the 51-mm-thick Type 304 stainless steel block, closer to the D-T neutron source. A sampling time of 50 s was applied to increase the net signal of the temperature rise. As noted in the Li_2CO_3 single-probe measurement, during the sampling interval, there should be appreciable changes in the temperature rise due to the finite heat outflow at the front surface of the block. The initial value of a temperature rise at the beginning of the pulse, therefore, was corrected by extrapolating the exponential-like curve of the profile to the corresponding initial point. The corrected heating rates are also plotted in Fig. 14. The discrepancy between the experiment and calculation was reduced significantly. This result clearly demonstrates that the heat transfer consideration is very essential in determining the heating rate when the large size detector is used. The general agreement between the calculation and the experiment suggests that the nuclear data of Type 304 stainless steel employed in this analysis seems adequate as long as the validity of the correction method is assured.

Figures 15 and 16 show differential sensitivities of neutron and gamma-ray nuclear heating at 15, 150, and 250 mm from the surface of the assembly, calculated by DOT3.5 with FUSION-J3. Here, the differential sensitivity is defined as the product of the neutron spectrum and the kerma factor. The D-T neutron peak fraction decreases with the depth appreciably, whereas the fraction of low-energy components are not so rapidly decreasing. In particular, the flux in the energy region below 100 keV doesn't change according to the position. Moreover, the neutron flux below 10 keV, on the contrary, increases as the depth increases. The fraction of 14-MeV neutrons at 215 mm becomes only 2% of the total neutrons. Thus, the nuclear heating rate at this position is mainly contributed by the low-energy neutrons. The neutron kerma of Type 304 stainless steel has, in general, a higher sensitivity with higher neutron energy. It is noted that the sensitivity of the 14-MeV neutrons still remains a larger fraction in the field at the 215-mm depth.

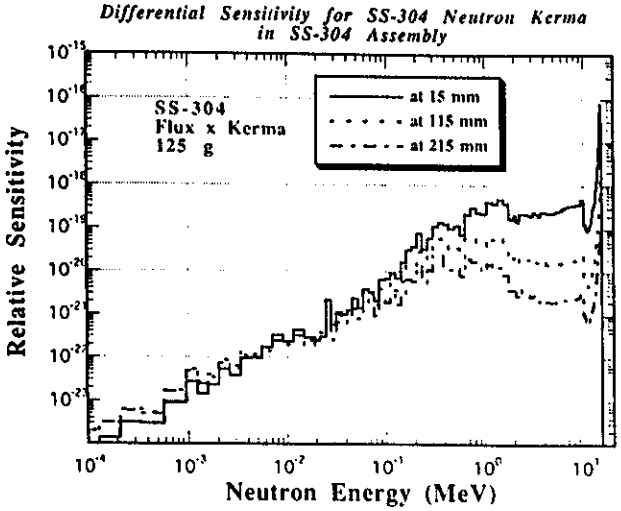

Fig. 15. Differential sensitivities of neutron heating rate for Type 304 stainless steel at 15, 115, and 215 mm from the surface of the Type 304 stainless steel assembly.

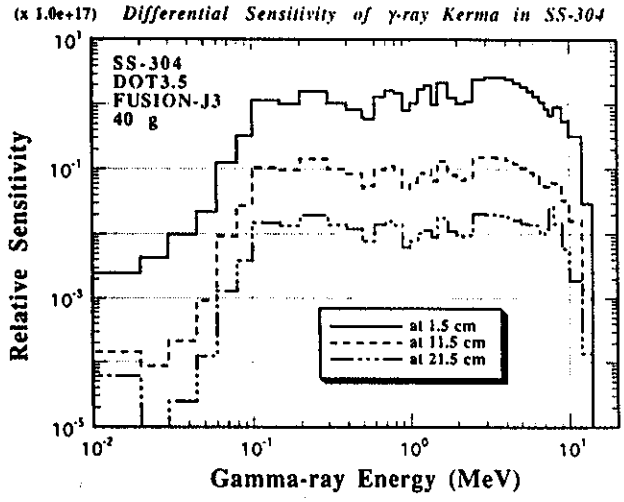

Fig. 16. Differential sensitivities of gamma-ray heating rate for Type 304 stainless steel at 15, 115, and 215 mm from the surface of the Type 304 stainless steel assembly.

Kerma factors of gamma-rays also have an ascending profile for almost all materials at an energy higher than several hundred kilo-electron-volts. At the energy below 100 keV, the kerma of gamma-rays increases greatly. However, the spectrum is dominated by the gamma-rays with energy ranging from hundreds of keV to 10 MeV; therefore, the low energy gamma-ray contribution is expected to be small. As seen in Fig. 14, emphasis should be placed on the situation that gamma-ray contribution to the heating rate becomes dominant as the depth of the position increases.

As regards the neutron and gamma-ray spectra at the deeper position of a shielding structure, they are very similar to those at 215 mm in this assembly. It is worthwhile to note that these experimental data are assumed to be the substantial data for the verification of the data and methods to be applied in the design calculation.

This study shows the possible direction of applying the calorimetric method on the total nuclear heating measurement for validating design calculations. However, the uncertainty in the nuclear heating at the deeper region, e.g., at the interface between the shield structure and the following insulator and superconducting magnet, largely depends on the uncertainty in the neutron and gamma-ray flux spectrum calculation. To arrive at the confidence levels of the design calculation uncertainty, the essential part in terms of neutron and gamma-ray flux spectrum determination should be concerned. More effort should be spent on the dosimetry study.

VI. CONCLUSION

Measurements of the nuclear heat deposition rate were carried out on six metallic structural materials of aluminum, titanium, iron, nickel, molybdenum, and Type 304 stainless steel, along with lithium carbonate, subjected to 14-MeV neutron fluxes. The measured data were compared with the calculations of the relevant currently available nuclear data. The calculations based on JENDL-3 and ENDL-85 gave better agreement with the experiments than calculations with RMCCS. The overall uncertainty range of ±30% was assured for the JENDL and ENDL-85 as long as the D-T neutron dominant field is concerned. It was demonstrated that the heat transfer calculation code ADINAT, coupled with DOT3.5, is effective to analyze the time-dependent profile of the nuclear heating rate in the medium with low thermal conductivity and a steep gradient in the heat source distribution.

The Type 304 stainless steel assembly experiment provided nuclear heating distribution data in depth up to 200 mm. It was suggested that a stronger neutron source and a more sensitive thermal detection system are required to measure data in the deeper region. However, as regards the neutron spectrum simulation of the field of interest in the shield design for fusion reactors, this type of integral experiment is very effective to validate the overall nuclear heating process. Although a further examination of the data is still needed in terms of reduction of uncertainty, these results demonstrate that calculations base don JENDL-3 are almost adequate within experimental error. In conclusion, the experimental approach with a microcalorimeter, demonstrated in this study, offers a more promising way to arrive at the production of experimental data for validating the adequacy of design calculations and associated nuclear data.

ACKNOWLEDGMENTS

The authors would like to express their sincere thanks to J. Kusano, C. Kutsukake, S. Tanaka, and Y. Abe for the operation of the FNS accelerator in the particular experimental request. The authors are grateful to T. Nakamura for his valuable advice and encouragement for the experimental program in the earlier stage. The work contributed by the United States was supported by U.S. DOE.

REFERENCES

1. M. A. ABDOU, C. W. MAYNARD, and R. Q. WRIGHT, "MACK: A Computer Program to Calculate Neutron Energy Release Parameters (Fluence-to-Kerma Factor) and Multigroup Reaction Cross Sections from Nuclear Data in ENDF Format," ORNL-TM-3994, Oak Ridge National Laboratory (July 1973).

2. M. A. ABDOU and C. W. MAYNARD, "Calculation Methods for Nuclear Heating—Part I: Theoretical and Computational Algorithms," *Nucl. Sci. Eng.*, **56**, 360 (1975).

3. M. A. ABDOU and C. W. MAYNARD, "Calculation Methods for Nuclear Heating—Part II: Applications to Fusion Reactor Blanket and Shields," *Nucl. Sci. Eng.*, **56**, 381 (1975).

4. Y. FARAWILA, Y. GOHAR, and C. W. MAYNARD, "KAOS/LIB-V: A Library of Nuclear Response Functions Generated by KAOS-V Code from ENDF/B-V and Other Data Files," ANL/FPP/TM-241, Argonne National Laboratory (1989).

5. K. MAKI, H. KAWASAKI, K. KOSAKO, and Y. SEKI, "Nuclear Heating Constant KERMA Library," JAERI-M 91-073, Japan Atomic Energy Research Institute (1991) (in Japanese).

6. M. KAWAI et al., "Review of the Research and Application of KERMA Factor and DPA Cross Section," JAERI-M 91-043, Japan Atomic Energy Research Institute (1991) (in Japanese).

7. A. KUMAR, Y. IKEDA, and C. KONNO, "Experimental Measurements and Analysis of Nuclear Heat Deposition Rates in Simulated D-T Neutron Environment: JAERI/USDOE Collaborative Program on Fusion Neutronics Experiments," *Fusion Technol.*, **19**, 1979 (1991).

8. A. KUMAR et al., "Direct Nuclear Heating Measurement in Fusion Neutron Environment and Analysis," *Fusion Eng. Des.* (to be published).

9. Y. IKEDA et al., "Measurement and Analysis for Nuclear Heat Depositions in Structural Materials Induced by D-T Neutrons," *Fusion Technol.*, **21**, 2190 (1992).

10. A. KUMAR et al., "Direct Nuclear Heating Measurements and Analyses for Plasma-Facing Materials," *Fusion Technol.*, **28**, 173 (1995).

11. T. NAKAMURA et al., "Present Status of the Fusion Neutron Source (FNS)," *Proc. 4th Symp. Accelerator Sci. Technol.*, Riken, Japan, November 24–26, 1982, p. 155.

12. S. R. DOMEN, "Advances in Calorimetry for Radiation Dosimetry," *The Dosimetry of Ionization*, Vol. II, K. R. KASE, B. E. BIANGRAD, and F. H. ATTIX, Eds., Academic Press, Orlando, Florida (1987).

13. S. R. GUNN, "Radio Calorimetric Calorimetry: A Review," *Nucl. Instrum. Methods*, **29**, 1 (1964); see also *Nucl. Instrum. Methods*, **85**, 285 (1970); see also *Nucl. Instrum. Methods*, **135**, 251 (1976).

14. S. R. DOMEN and P. J. LAMPERTI, "A Heat-Loss-Compensated Calorimeter: Theory, Design and Performance," *J. Res. Nat. Bur. Stand. (U.S.) (Phys. and Chem.)*, **78A**, *5*, 595 (1974).

15. J. S. LAUGHLIN and S. GENNA, "Calorimetry," *Radiation Dosimetry*, Vol. II, F. H. ATTIX and W. C. ROESCH, Eds., Academic Press, New York (1966).

16. J. A. MASON, A. N. ASFAR, and P. J. GRANT, "Improved Microcalorimetry for Radiation Absorbed Dose Measurement," *Proc. 5th Symp. Reactor Dosimetry*, Vol. 1, p. 415, American Society for Testing and Materials/Euratom (1984).

17. K. SHIBATA et al., "Japanese Evaluated Nuclear Data Library, Version-3," JAERI-1319, Japan Atomic Energy Research Institute (1990).

18. "MCNP—A General Monte Carlo Code for Neutron and Photon Transport: Version 3A," LA-7396-M, Rev. 2, Los Alamos National Laboratory (1988); see also "MCNP3B Newsletter," J. F. BREISMEISTER, Ed., Los Alamos National Laboratory (July 18, 1988).

19. R. J. HOWERTON, "Calculated Neutron Kerma Factors Based on the LLNL ENDL Data File," UCRL-50400, Vol. 27, University of California, Berkeley (1986).

20. "ADINAT, A Finite Element Program for Automatic Dynamic Incremental Nonlinear Analysis of Temperature," ADINA Engineering (1984).

21. Y. S. TOULOUKIAN and E. H. BUYCO, *Specific Heat: Metallic Elements and Alloys*, Vol. 4 of a Series on Thermophysical Properties of Matter, IFI/Plenum, New York (1970); see also *Specific Heat: Nonmetallic Solids*, Vol. 5 of the series, IFI/Plenum, New York (1970).

22. Y. IKEDA et al., "Joint Report of JAERI/USDOE Collaboration on Fusion Neutronics—Nuclear Heating Experiment," Japan Atomic Energy Research Institute (to be published).

23. Y. OYAMA et al., "Phase-II C Experiments of the JAERI/USDOE Collaborative Program on Fusion Blanket Neutronics—Experiments and Analysis of the Heterogeneous Fusion Blankets," Vol. I, JAERI-M 92 182, UCLA-FTN-63, UCLA-ENG-93-18, University of California, Los Angeles (1992).

24. M. NAKAGAWA et al., "Phase-II C Experiments of the JAERI/USDOE Collaborative Program on Fusion Blanket Neutronics—Experiments and Analysis of the Heterogeneous Fusion Blankets," Vol. II, JAERI-M 92-183, UCLA-FTN-64, UCLA-ENG-93-19, University of California, Los Angeles (1992).

25. H. MAEKAWA, Y. IKEDA, Y. OYAMA, S. YAMAGUCHI, and T. NAKAMURA, "Neutron Yield Monitors for the Fusion Neutronics Source (FNS)," JAERI-M 83-219, Japan Atomic Energy Research Institute (1983).

26. Y. IKEDA et al., "Absolute Measurements of Activation Cross Sections of $^{27}Al(n,p)^{27}Mg$, $^{27}Al(n,\alpha)^{24}Na$, $^{56}Fe(n,p)^{56}Mn$, $^{90}Zr(n,2n)^{89m+g}Zr$ and $^{93}Nb(n,2n)^{92m}Nb$ at an Energy Range of 13.3 ~ 14.9 MeV," *J. Nucl. Sci. Technol.*, **30**, *9*, 870 (1993).

27. W. A. RHOADES and F. R. MYNATT, "The DOT III Two-Dimensional Discrete Ordinates Transport Code," ORNL/TM-4280, Oak Ridge National Laboratory (1979).

28. K. MAKI, K. KOSAKO, Y. SEKI, and H. KAWASAKI, "Nuclear Group Constant Set FUSION-J3 for Fusion Reactor Nuclear Calculations Based on JENDL-3," JAERI-M 91-072, Japan Atomic Energy Research Institute (1991).

29. R. E. MacFARLANE, D. W. MUIR, and R. M. BOICOURT, "The NJOY Nuclear Data Processing System, Volume II: The NJOY, RECONR, BROADR, HEATR and THERMR Modules," LA-9303-M, Vol. II (ENDF-324), p. 19, Los Alamos National Laboratory (1982); see also R J. HOWERTON, "Calculated Neutron Kerma Factors Based on the LLNL ENDL Data File," UCRL 50400 Vol. 27, University of California, Berkeley (Jan. 1986).

30. R. W. ROUSSIN, J. R. KNIGHT, J. H. HUBBELL, and R. J. HOWERTON, "Description of DLC-99/HUGO Package of Photon Interaction Data in ENDF/B-V Format," ORNL/RSIC-46 (ENDF-335), Oak Ridge National Laboratory (1983).

31. R. MacFARLANE, "Energy Balance of ENDF/B-V," *Trans. Am. Nucl. Soc.*, 33, 681 (1979).

Yujiro Ikeda (PhD, nuclear engineering, Nagoya University, Japan, 1981) is head of the Fusion Neutronics Laboratory in the Department of Reactor Engineering at the Japan Atomic Energy Research Institute (JAERI). He has worked in the areas of fusion neutronics experiments, induced radioactivity experiment and analysis, direct nuclear heating measurements, activation cross-section measurements, and fusion dosimetry.

Anil Kumar (PhD, University of Bombay, India, 1981) is senior development engineer at the University of California, Los Angeles (UCLA). His current research interests include fusion reactor nucleonics experiments and analysis, technique development for nuclear heating, decay heat measurements, biological dose, fusion diagnostics, safety factor methodology for fusion reactor design parameters, low-activation materials, inertial confinement fusion, and sequential reactions. He has conducted experiments at leading facilities such as the Fusion Neutronics Source (FNS) facility in Japan, the Tokamak Fusion Test Reactor (TFTR) at Princeton University, and LOTUS in Switzerland.

Chikara Konno (MS, physics, Kyoto University, Japan, 1985) is a research scientist in the Department of Reactor Engineering at JAERI. He has worked in the areas of fusion neutronics experiments, cross-section measurements, and neutron spectrum measurements using a proton-recoil counter.

Kazuaki Kosako (BE, atomic engineering, Tokai University, Japan, 1984) has worked at Sumitomo Atomic Energy Industries since 1994. He worked in the Department of Reactor Engineering at JAERI from 1984 to 1992 where he was involved mainly in fusion neutronics. He is currently interested in the area of radiation damage of materials.

Yukio Oyama (BS, physics, 1975, MS, nuclear physics, 1977, Dr. Eng., 1989, Osaka University, Japan) is a principal scientist at JAERI. He has worked in the area of fusion neutronics experiments since 1978. He is currently involved in intense and high-energy neutron source projects.

Fujio Maekawa (MS, nuclear engineering, Osaka University, Japan, 1990) is a research scientist at JAERI. He has been engaged in integral experiments for fusion neutronics and studied the behavior of neutron, photon, and electron

transport in media. His current interests are in the measurements of tritium and decay heat of irradiated materials.

Hiroshi Maekawa (BE, 1965; MS, 1967; and Dr. Eng., 1970, nuclear engineering, Tokyo Institute of Technology, Japan) is the deputy director of the Department of Reactor Engineering and the head of the Intense Neutron Source Laboratory at JAERI. He has worked on fusion neutronics for more than 20 years, and he planned and constructed the FNS facility. He served as the Japanese leader of the JAERI/U.S. Department of Energy (U.S. DOE) collaboration on fusion blanket neutronics. His recent research has focused on International Fusion Materials Irradiation Facility conceptual design activities.

Mahmoud Z. Youssef (PhD, nuclear engineering, University of Wisconsin, 1980) is a senior research engineer in the Department of Mechanical, Aerospace, and Nuclear Engineering at UCLA. He participated in several conceptual magnetic fusion energy and inertial fusion energy reactor design studies with emphasis on nuclear analysis and blanket/shield design. His research interests are in the areas of blanket/shield design optimization, nuclear data, sensitivity/uncertainty studies, neutronics methods and code development, tritium fuel cycle, radioactivity and safety aspects of fusion, integral experiments, neutronics testing, and research and development for fusion reactors, particularly the International Thermonuclear Experimental Reactor (ITER).

Mohamed A. Abdou is a professor in the Department of Mechanical, Aerospace, and Nuclear Engineering at UCLA and also is the director of fusion technology at UCLA. His research interests include neutronics, thermomechanics, fusion technology, and reactor design and analysis. He served as the U.S. leader of the JAERI/U.S. DOE collaboration on fusion blanket neutronics.